Dissolution does not affect grass phytolith assemblages

Hongye Liu, Jean-Dominique Meunier, Olivier Grauby, Jérôme Labille, Anne Alexandre, Doris Barboni

Dissolution does not affect grass phytolith assemblages

Hongye Liu[a, b, *], Jean-Dominique Meunier[a], Olivier Grauby[c], Jérôme Labille[a], Anne Alexandre[a], Doris Barboni[a, d]

[a] *CEREGE, Aix-Marseille Université, CNRS, IRD, INRAE, Aix en Provence, France*

[b] *State Key Laboratory of Biogeology and Environmental Geology, China University of Geosciences, Wuhan 430074, China*

[c] *Aix-Marseille Université, CNRS, CINaM, Marseille, Cedex 09, France*

[d] *Institut Français de Pondichéry, UMIFRE 21, UAR 3330 « Savoirs et Mondes Indiens », Pondicherry, India*

[*] Corresponding author: hoyeliu@cug.edu.cn – Hongye LIU, China University of Geosciences, Lumo Rd. 388, Wuhan 430074, China.

Abstract

Dissolution is one among several taphonomical processes that may bias paleoenvironmental, paleoclimatic or taxonomic interpretation of phytolith assemblages. To improve our understanding of dissolution on grass phytoliths, we studied systematic changes of surface features, morphotype assemblages, and dissolution rates of phytoliths extracted from two grass species *Hyparrhenia involucrata* (Panicoideae), *Nastus borbonicus* (Bambusoideae), one soil from La Réunion Island (approximate mean age < 800 yr), and three paleosols from Ethiopia (approximate age of 4.4 million years). We used heavy-liquid to extract phytoliths, and 1% Na_2CO_3 to perform partial dissolution experiments. Physicochemical surface properties, morphotypes, and assemblages were analyzed using optical and scanning electron microscopy, laser diffraction, and X-ray diffractometry. Our results show that 1) phytoliths from different grass species may have different dissolution rates: phytoliths from the leaves of *Hyparrhenia involucrata* (Panicoideae) are more prone to dissolution than those from *Nastus borbonicus* (Bambusoideae). 2) Silicon (Si) released by phytolith assemblages (i.e., phytolith dissolution rate) decreases as follows: plant > soil > paleosol. 3) Dissolution leads to cavity formation on phytolith surfaces and disappearance of fragile silica particles. 4) Partial dissolution does not significantly change percentages of common grass phytolith

morphotypes in a given assemblage. These results provide a benchmark for assessing the reliability of paleoenvironmental reconstructions using grass phytolith assemblages from buried soils and sediments.

Keywords: weathered phytolith, dissolution, stability, pH, paleoenvironment

1. Introduction

Phytoliths are extensively used in paleobotany (e.g., Piperno and Pearsall, 1998; Prasad et al., 2011), archaeobotany (e.g., Ball et al., 2016; Lu et al., 2009, 2016), paleoenvironmental and paleoclimatic studies (e.g., Arráiz et al., 2017; Issaharou-Matchi et al., 2016; Nogué et al., 2017; Yost et al., 2021; Zhang et al., 2020). They are produced in stems and leaves of many plants (Hodson et al., 2005), and are particularly abundant, taxonomically diagnostic, and precisely classified within grasses (Poaceae) (Piperno, 2006). Grass phytolith assemblages can provide detailed information about the composition of past grass flora (e.g., Bremond et al., 2008; Cordova et al., 2011; Fredlund and Tieszen, 1994). Phytolith ratios, particularly those including grass silica short cells (GSSCs), have been used as climatic proxies to track paleoclimate changes (e.g., Aleman et al., 2014; Nogué et al., 2017; Zhang et al., 2020).

Using buried soil or sedimentary phytolith assemblages to reconstruct past environments assumes that they reflect some of their source vegetation characteristics (e.g., tree cover density, grass subfamily dominance, grass drought stress), despite dissolution and concentration mechanisms known to affect phytoliths in litters, soils, surface waters and sediments (Alexandre et al., 2011; Hyland et al., 2013; McCune et al., 2013). In terrestrial ecosystems, phytoliths can be highly soluble and recycled (e.g., Meunier et al., 2022), with concentations in soils decreasing with increasing depth: highest at the surface, decreasing below about 30-80 cm, and stabilizing in deeper horizons (Alexandre et al., 1997; White et al., 2012), implying the occurrence of phytolith dissolution and/or translocation during pedogenesis (Alexandre et al., 2011).

Phytoliths are among the fastest dissolving silicate constituents in soil at pH > 4; pH > 8-9 amplifies their solubility (Fraysse et al., 2009), making the phytolith preservation problematic in alkaline soil and sediments (e.g., Arráiz et al. 2017; Liu et al., 2019; Yost et al., 2021). Conversely,

phytoliths may accumulate in acidic environments (Meunier et al., 1999; Nguyen et al., 2019), and preserve well in sedimentary contexts oversaturated with silica (e.g., Novello et al., 2015). Several experimental tests demonstrated that phytoliths from fresh plants are more soluble than those from fossil plants (Cabanes et al., 2011; Cabanes and Shahack-Gross, 2015), supporting the hypothesis that only a portion of phytoliths incorporated into soil are preserved for long periods. These tests also indicated that thin and flat phytoliths with large surface area relative to volume (e.g., Double-peaked husk phytoliths from rice, Papillate phytoliths from sedges) are more likely to dissolve than thick, densely silicified particles such as grass silica short cell phytoliths (e.g., Bartoli and Wilding, 1980; Cabanes et al., 2011), suggesting that preferential dissolution may be problematic because paleovegetation inferences rely on the relative abundance of phytolith morphotypes.

In soils and sediments, phytoliths do not always have a smooth, pristine surface. They often exhibit cavities that are round, deep and large, suggesting dissolution pits. Phytoliths with numerous cavities are particularly abundant at lower soil profile depths, even under soil with acidic to neutral conditions (Borrelli et al., 2010; Riotte et al., 2018). Dissolution processes may affect the surface of phytoliths to the point that taxonomic identification is impossible (e.g., Arráiz et al., 2017; Cabanes et al., 2011; Yost et al., 2021).

Given that grass phytoliths are exceptional tools used in paleoecology and archaeobotany to document past grass communities, changes in herbivore diets (e.g., Ciochon et al., 1990), early domestication of cereals (e.g., Iriarte, 2003; Zhao and Piperno, 2000), changes in agricultural practices (e.g., irrigation; Rosen and Weiner, 1994), as well as understanding the contribution of plants to the global silicon cycle (Alexandre et al., 1997, 2011; Blecker et al., 2006; Borrelli et al., 2010), improved understanding of effects of dissolution and other taphonomic processes on grass phytolith assemblages is crucial.

To improve our understanding of the impact of dissolution processes on grass phytolith morphotypes and assemblages, we performed laboratory experiments simulating alkaline dissolution. Phytolith sensitivity to dissolution was evaluated by measuring Si release from phytoliths extracted from two tropical grass species, one sub-modern soil sample with abundant bamboo phytoliths (Meunier et al., 1999), and Pliocene paleosol samples containing high grass and palm (Arecaceae) phytoliths (WoldeGabriel et al., 2009). For the first time, effects of partial

dissolution on phytolith surfaces are described and quantified for different morphotypes originating from different silicification processes (Hodson, 2019). Impacts on phytolith assemblages were also assessed through morphotype counts and quantification of altered surfaces.

2. Materials and methods

2.1 Plant, soil and paleosol samples

Plant phytoliths were extracted from two grass species: a specimen of *Hyparrhenia involucrata* (Panicoideae) collected in 2018 as part of the HUMI-17 project at the Nalohou grassland site at the AMMA-CATCH observatory (www.amma-catch.org) in Benin (9°44'N, 1°36'E) (Outrequin, 2022), and a specimen of *Nastus borbonicus* (Bambusoideae) collected from La Réunion Island (21°07'S, 55°32'E) (Meunier et al., 1999).

The soil sample was collected at 20 cm depth in the M horizon of an Andosol developed on the west side of La Réunion Island, which is mostly covered by bamboo forests; estimated sample age is 745 years (charcoal ^{14}C age, Meunier et al., 1999). Paleosol samples (SA18, SA28, and SA52) with relatively abundant phytoliths were obtained from the Sagantole Formation in the Middle Awash Valley of Ethiopia and are dated ca. 4.4 Ma (10.5°N, 40.5°E, WoldeGabriel et al., 2009).

2.2 Phytolith extraction

Plant phytoliths were extracted using a wet oxidation method (Alexandre et al., 1997). Leaves were separated from stems, washed, dried at 50°C, and cut into small pieces. Milli-Q ultrapure water was used for rinsing. Dried pieces of leaves were soaked in 1N HCl and heated at 80°C for 2 h, rinsed, soaked in H_2SO_4 (95%) and heated at 80°C for > 8h. To improve oxidation of organic matter, samples were soaked again in H_2O_2 (30%, at 80°C) until the supernatant became clear. Samples were then rinsed, centrifuged (10 min at 4000 rpm), and dried before storage. Plant phytolith content, expressed as a percentage relative to plant leaf dry biomass (% DW), was 4.4% in *Hyparrhenia involucrata* and 12.8% in *Nastus borbonicus* (Table S1).

Chemical extraction may cause some dissolution (Crespin et al., 2008), so, we used the same protocol for all our samples to avoid the bias shown by Cabanes et al. (2011), who used dry ashing and acid digestion.

Soil and paleosol phytoliths were extracted using the protocol of Alexandre et al. (1997). No treatment was needed for the La Réunion soil sample because it is almost exclusively composed of phytoliths (Meunier et al., 1999). Phytoliths were extracted from paleosol samples using 1N HCl heated at 80°C for 2 h to remove carbonates and 30% H_2O_2 under constant heat (80°C) to remove organic matter. Clays were removed by decantation, and minerals by densimetric separation using $ZnBr_2$ heavy liquid with density 2.3 g/cm^3.

After extraction, phytolith extracts were weighed and three to five permanent slides were prepared with Canada Balsam for microscopic observation. The remaining extract was used for dissolution experiments and scanning electron microscope (SEM) observations.

2.3 Phytolith dissolution experiments and Si measurement

Phytoliths were subjected to partial dissolution using 1% Na_2CO_3 solution. Sixty mg dried phytolith powder were added to 100 ml 1% Na_2CO_3 solution (pH = 11.2) in a polypropylene tube with caps slightly loosened to vent gases, and placed in a shaker bath at 85 °C for digestion. To stop the reaction, the tube was cooled in a water bath at room temperature. To measure dissolved Si, 1ml liquid aliquot was added to 9 ml 0.021 N HCl in 10 ml polypropylene tubes, washed in 0.1mol/l HCl (twice) and Milli-Q ultrapure water (twice), centrifuged for 10 min at 4000 rpm, and dried at 70°C for weighing and phytolith observation.

Dissolution times had to be adjusted for each sample (Table S1). At ½ hour, phytoliths were partially dissolved in *Hyparrhenia* and *Nastus*, while they were barely affected in the soil and paleosol samples. Dissolution times were increased for the soil (up to 4h) and paleosol samples (up to 10 days) to obtain noticeable dissolution. We duplicated the plant and La Réunion soil samples to test the reproducibility of the dissolution experiment and error values were calculated as the standard deviation between duplicates. For the paleosol samples, instead of duplicating the experiments, which was not possible due to the small amount of material available, we chose three different samples (SA18, SA28, SA52) of similar age (WoldeGabriel et al., 2009) and treated them separately. Because they originated from the same geological Formation but from different localities within the same paleontological area where paleovegetation was likely different.

Concentration of dissolved Si (DSi, mg L^{-1}) in solution was measured using molybdenum blue colorimetry with Spectroquant reactants (Merck), which allows monitoring the phytolith dissolution process with coefficient of variation ± 1.4%. Absorption was detected at 820 nm with a Jasco V-650 Spectrometer. Calibration lines ($R^2 \geq 0.999$) were calculated using dilute solutions from a standard Si solution at 1g L^{-1} (Plasma CAL).

Percent phytolith dissolution was estimated using two methods: 1) calculating Si loss in solution according to the following equation:

$$Phy_{loss\text{-}DSi}\ (\%) = DSi\ (mg\ L^{-1}) \times 0.1\ (L) \times 10 / \text{initial phytolith weight (mg)} / 0.42 \times 100$$

where 10 is the dilution of 1 ml liquid aliquot in 9 ml 0.021 M HCl, 0.1 (liter) is the volume of Na_2CO_3 solution, in which the sample was digested, and 0.42 corresponds to 42% mass of Si in phytoliths; 2) estimating the percentage of phytoliths dissolved based on phytolith mass remaining after dissolution:

$$Phy_{loss\text{-}phy}\ (\%) = (\text{initial phytolith mass (mg)} - \text{final phytolith mass (mg)}) / \text{initial phytolith mass (mg)} \times 100$$

Data are presented in Table S1 for all experiments. However, after 10 days, solution volume was different from the initial volume, so $Phy_{loss\text{-}DSi}$ could not be calculated accurately.

2.4 Counting, observation and properties of phytolith assemblages

Identification, observation, and counting of phytoliths was performed at ×400 and ×600 magnification with an optical microscope. Phytolith names follow the International Code for Phytolith Nomenclature 2.0 (Neumann et al, 2019). We identified and counted the most common and stable morphotypes present in soil and paleosol phytolith assemblages. SADDLE (SAD), BILOBATE (BIL) and RONDEL (RON) are GSSCs diagnostic of Poaceae. BULLIFORM FLABELLATE (BUL-FLA) is diagnostic of Poaceae and Cyperaceae. SPHEROID ECHINATE and SPHEROID

DECORATED (SPH) are diagnostic of Arecaceae and woody taxa, respectively. Other common morphotypes such as ELONGATE (ELO), ACUTE BULBOSUS (ACU-BUL) and BLOCKY (BLO) have no taxonomical value. We did not count rare morphotypes and fragile particles such as small and thin (< 5 µm) silica pieces with ill-defined shapes, and silicified stomata. More than 500 phytoliths were counted over several slides and phytolith morphotype percentages were calculated.

Exact Clopper-Pearson confidence intervals (95% CIs) were calculated for each phytolith morphotype percentage (Suchéras-Marx et al., 2019). Contingency table analysis, with p values from the chi-squared distribution and from a permutation test with 9999 replicates, was used to test whether the dissolution significantly altered phytolith assemblages (Davis, 1986). The null hypothesis H0 is that assemblages are similar at $p > 0.05$ (i.e. dissolution is not significant). When $p \leq 0.05$, changes in assemblages can be confirmed. Both 95% CIs on proportions and Chi-square tests on counts were calculated using PAST (Hammer et al., 2001).

Several terminologies have been used to describe weathered phytoliths. Here we used 'cavity' (Lisztes-Szabó et al., 2020), which is equivalent to 'pits' or 'pitted surface' (Cabanes et al., 2011) and 'cratered phytoliths' (Kaczorek et al., 2019). To evaluate weathering intensity, we classified unweathered phytoliths as 'smooth' when the surface was smooth and devoid of cavities, 'irregular' when the surface looked dark and rough without evident cavities under the microscope, 'moderately weathered' when cavities occupied less than 50% of the phytolith surface, and 'highly weathered' when cavities could be observed on more than 50% of the phytolith surface.

In addition to light microscopy, we carried out a grain size analysis of each pure phytolith sample obtained from the plants before and after dissolution experiments using laser diffraction (Mastersizer 3000, Malvern Panalytical) to test the hypothesis that fragile silica particles and/or smaller phytoliths were preferentially dissolved. Phytolith samples were dispersed in pure water without additional physical (crushing) treatment to avoid breaking silica particles and magnetically agitated to keep them in suspension during measurement. Analyses were made in triplicate and averaged.

We also performed X-ray diffraction (PANanalytical X'Pert Pro X-ray diffractometer; Co anti-cathode, 40KV; 40mA) on ground phytolith powders to analyze mineral composition of plant *Nastus borbonicus*, La Réunion soil, and the paleosol SA18. Phytoliths were mounted on stubs

using double-sided carbon tape for further surface analysis using scanning electron microscopy equipped with energy dispersive X-ray (EDX) for localized element analysis (SEM, JEOL JSM-7900 F × Flash 60-Brüker).

3. Results

3.1 Physical, mineralogical and chemical characteristics resulting from partial dissolution

Before dissolution tests we observed that phytoliths from plants, soil, and paleosol samples exhibit important differences at different levels. First, XRD analysis showed mineral composition of phytolith assemblages extracted from *Nastus borbonicus* leaves and La Réunion soil peak at 2-theta value 25°, indicating only opal-A with no well-defined crystalline structure (Figs. S1a-b). Pliocene paleosols, on the other hand, include small amounts of crystalline mineral residues such as quartz, smectite, cristobalite and tridymite despite the careful extraction protocol (Fig. S1c). Second, Si and O were detected in all phytolith samples, but Al only on paleosol phytoliths (Fig. 1). C detected in all samples likely originated from the C coating used prior to SEM observations. Third, differences were found in grain-size distributions of pure phytoliths extracted from plants. Phytolith size distributions in undissolved assemblages of *Hyparrhenia involucrata* ranged from 1 to 200 µm, showing two overlapping populations centered at 2 µm and 10 µm, while *Nastus borbonicus* phytoliths ranged from 2 to 2,000 µm, showing two populations centered at 10-20 µm and 500 µm (Fig. 2). We assume that particles > 300 µm in the latter sample probably correspond to aggregates because phytoliths of this size were not observed in microscopy.

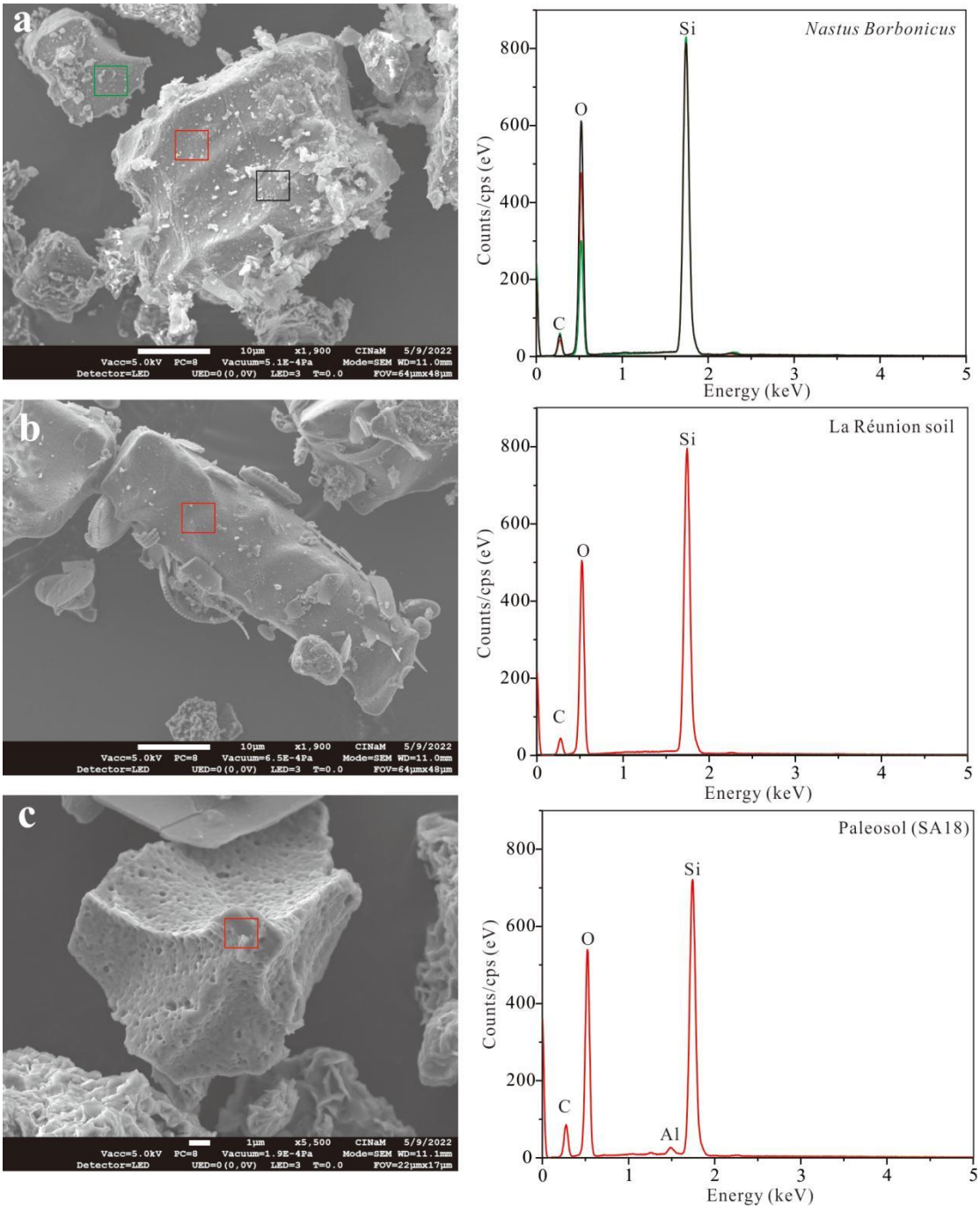

Fig. 1. SEM images and Energy dispersive X-ray spectroscopy of phytoliths before dissolution from a) *Nastus borbonicus* leaves, b) La Réunion soil, and c) paleosol SA18.

After partial dissolution treatment, grain-size distributions were less widespread (Fig. 2) mostly due to disappearance of particles < 2-5 µm originally seen in the assemblage from *Hyparrhenia involucrate* (Fig. S2), leaving only a narrow, monomodal distribution centered at 10 µm. The *Nastus* phytolith assemblage distribution remained bimodal but the low size peak was slightly shifted toward larger sizes, showing a new mode at 30 µm, likely due to dissolution of thin and small silica

particles that were present before the dissolution step (Fig. S2). Large phytolith aggregates comprising the upper end of the *Nastus borbonicus* size distribution showed lower maximum size after dissolution, likely because of aggregate separation.

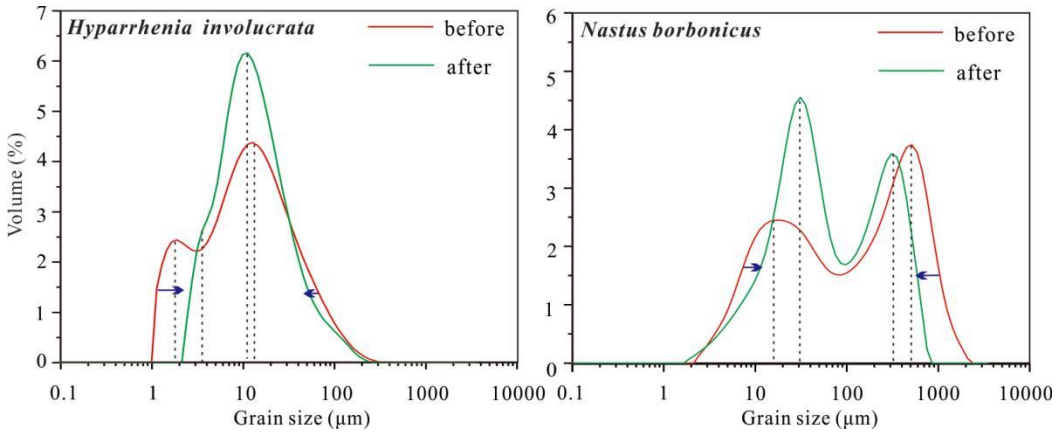

Fig. 2 Changes in the grain size distribution of phytolith assemblages from plants before and after dissolution.

Loss of phytoliths resulting from the dissolution experiments was also shown by values of Phy $_{loss\text{-}phy}$ and Phy $_{loss\text{-}DSi}$ (Fig. 3a), which showed a strong positive correlation ($R^2 = 0.95$, $p < 0.001$). Systematically lower values of Phy $_{loss\text{-}DSi}$ compared to Phy $_{loss\text{-}phy}$ indicate larger loss when considering phytolith mass for the calculation, possibly due to phytolith losses occurring during processing, particularly when the solution is removed after alkaline extraction. After ½ hour of dissolution, Phy $_{loss\text{-}DSi}$ was 44% to 80% for plants (phytoliths from leaves of *Hyparrhenia involucrata* dissolved more than those from *Nastus borbonicus*), and about 10% for soil and paleosols samples (Fig. 3b). The difference between Phy $_{loss\text{-}DSi}$ to Phy $_{loss\text{-}phy}$ was least for *Hyparrhenia involucrata* (+ 13%), followed by *Nastus borbonicus* (+44%), La Réunion soil (+90%), and paleosols (+170%). By extending dissolution times, we observed different behaviors between La Réunion soil and Pliocene paleosols. After 4 h, Phy $_{loss\text{-}DSi}$ was around 75% for La Réunion soil, close to results at ½ h for *Hyparrhenia involucrata* leaves. However, paleosol phytoliths remained little dissolved even after 16 h (Phy $_{loss\text{-}DSi}$ around 10%).

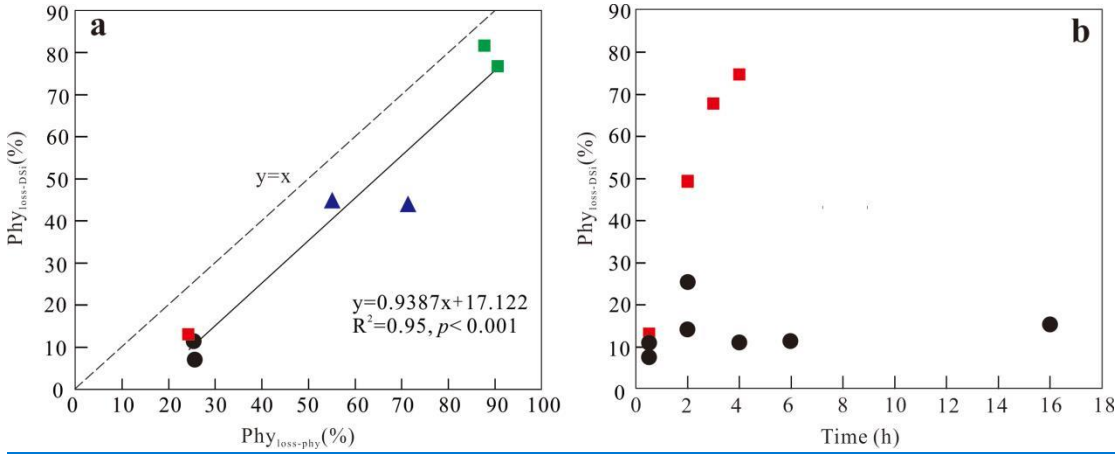

Fig. 3. Dissolution experiments of phytoliths in 1% $NaCO_3$ (60mg/100ml). a) Correlation between the percentages of phytolith loss from mass differences (Phy $_{loss-phy}$) and from Si measurement in solution (Phy $_{loss-DSi}$) after ½ hour; b) Phy $_{loss-phy}$ vs time. Green square = *Hyparrhenia involucrata* leaf, blue triangle = *Nastus borbonicus* leaf, red square = La Réunion soil, black round = Pliocene paleosol.

3.2 Visible dissolution features

Microscopic observation before dissolution showed differences on surfaces of phytoliths from plant, soil, and paleosol samples and as well as among phytoliths within a given assemblage. Phytoliths extracted from living plant tissues exhibited mostly smooth surfaces devoid of cavities. Spheres of around 100 nanometers were observed on the surface of some morphotypes using SEM (Fig. S3). On some BLOCKY and ELONGATES, however, rough and dark features over the whole phytolith surface were observed (Fig. 4). Some morphotypes in the La Réunion soil sample exhibited cavities (Fig. 4). In paleosol samples SA18 and SA28, coalescent cavities were seen on most morphotypes (Fig. 5).

Fig. 4 Surface properties changes of different phytolith morphotypes from plant and soil samples. Before dissolution, plant phytolith surfaces are smooth or irregular and some cavities can be observed on soil phytoliths, but after dissolution phytolith surfaces exhibit more cavities which have been categorized into moderately weathered (% cavities < 50%) or highly weathered (% cavities > 50%). m-w: moderately weathered, h-w: highly weathered.

After partial dissolution in 1% Na_2CO_3, we observe that thinly silicified cell walls, cuticles, shapeless and indefinite pieces of silica, as well as the silicified stomata present in plant phytolith samples have mostly disappeared (Fig. S2), while larger and more numerous cavities up to 20-30 µm diameter have appeared on surfaces of all plant, soil and paleosol phytoliths (Figs. 4-5). Dissolution altered surface of most grass morphotypes in paleosols but had little impact on SPHEROIDs produced by Arecaceae (palms) (Fig. 5).

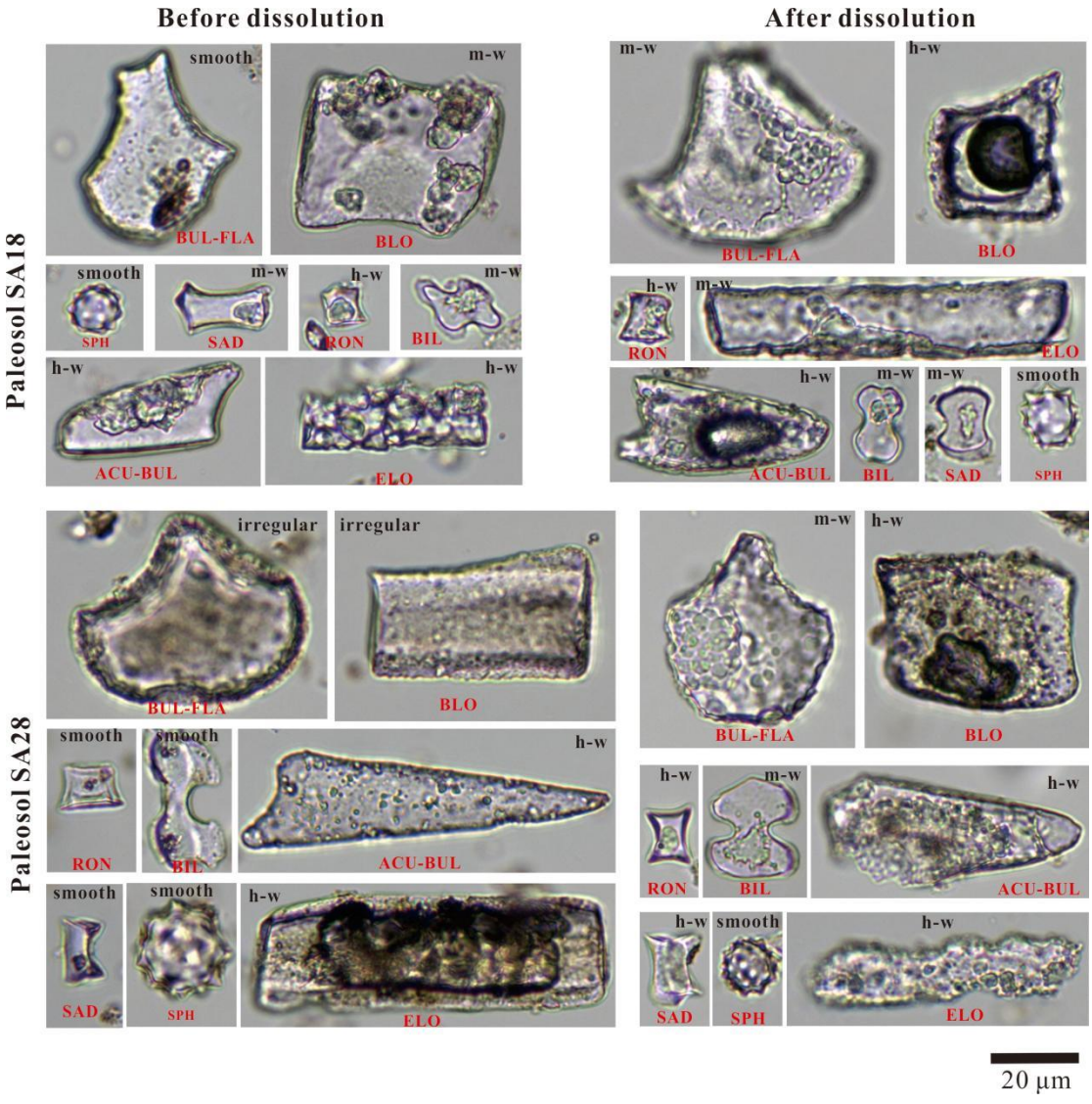

Fig. 5 Effects of dissolution on surface properties of different phytolith morphotypes from two Pliocene paleosol samples.

Before dissolution, paleosol phytolith surfaces already exhibited cavities, but after dissolution cavities are more numerous and larger. m-w: moderately weathered, h-w: highly weathered.

3.3 Impact of partial dissolution on the phytolith assemblages

After the partial dissolution experiments, well-defined phytolith morphotypes BUL-FLA, BLO, RON, SAD, BIL, ELO, ACU-BUL and SPH were still numerous and recognizable enough to identify and count despite sometimes highly weathered surfaces. Percentages of irregular, moderately and highly weathered morphotypes increased in all plant, soil and paleosol samples. In plant samples, moderately and highly weathered morphotypes represented 0-3% before dissolution, and up to 87% in *Hyparrhenia* and 72% in *Nastus* after partial dissolution, with almost no RON, BIL, SAD and ELO left intact (Figs. 6a-b).

Soil and paleosol phytoliths exhibited some cavities before dissolution; after dissolution relative proportions of highly weathered morphotypes increased >27% in La Réunion soil and >20% in paleosol sample SA28 (Figs. 6c-d). Increasing dissolution time increased the proportion of highly weathered morphotypes in paleosol sample SA18 from 76% to 84% and then to 90% (Fig. 6e). However, most SPH phytoliths were remained intact (Figs. 6d-e). As shown by overlapping percentage values and error bars, there were no significant differences between relative abundance of morphotypes in any assemblage, dissolution also did not alter assemblages according to a chi-squared test ($p > 0.05$) before and after partial dissolution (Fig. 6), but phytolith surfaces changed, becoming more deeply perforated (Figs. 4-5).

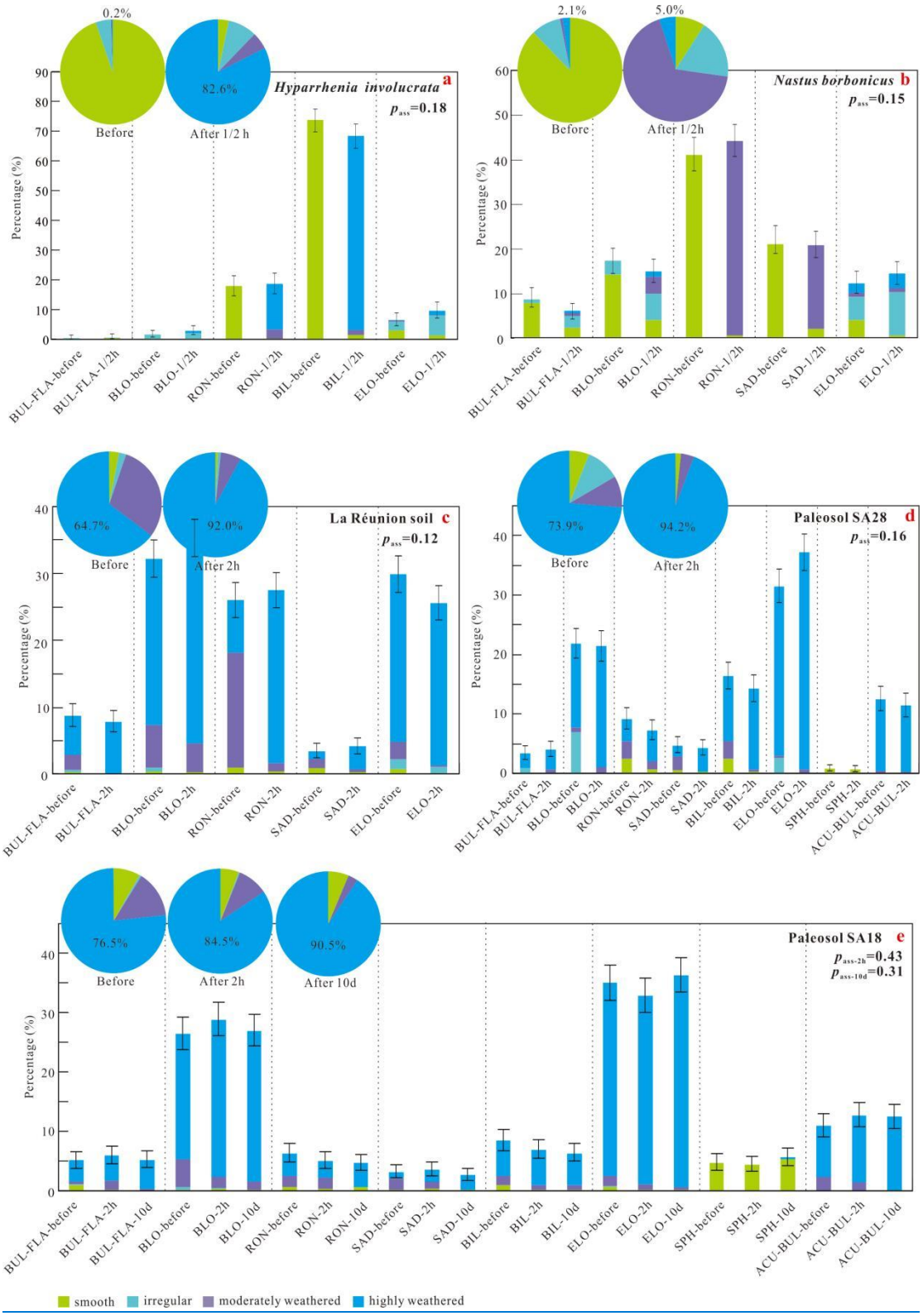

Fig. 6 Phytolith assemblages of the main morphotypes before and after partial dissolution experiments according to morphotypes (bar diagrams) and features on their surfaces (pie diagrams). Phytolith surfaces are defined as smooth, irregular, moderately weathered, and highly weathered. In each graph, the pie diagram at the far left shows proportions before dissolution times of ½ h for plants, 2 h for soil, and 2h and 10 days for paleosol samples.

$p > 0.05$ means no significant changes in phytolith assemblages (p_{ass}) before and after partial dissolution.

Discussion

4.1 Effects of dissolution on phytoliths

Our analysis showed that phytolith dissolution in 1% alkaline solution produces cavities on phytolith surfaces similar to features occurring naturally, as well as to features observed during dissolution experiments using different solutions (Cabanes et al., 2011; Kaczorek et al., 2019; Lisztes-Szabó et al., 2020), suggesting that our experiments mimic natural dissolution processes occurring in various sedimentary and pedological contexts. Dissolution of amorphous silica also occurs in acidic conditions, though acidic conditions compared to alkaline conditions are more favorable to phytolith preservation. Moreover, many soil phytoliths are likely to be preserved in organo-mineral aggregates, which we did not address in this study.

We observed that thin and small silica particles, very abundant in leaves of *Hyparrhenia involucrata* and *Nastus borbonicus*, disappeared after experimental dissolution (Fig S2), more so in the phytolith assemblage of *Hyparrhenia* compared to *Nastus* (Figs. 2-3). Comparing grain size evolution of the two plant phytolith assemblages showed that dissolution of the smallest particles (< 2mm) and disaggregation of the largest aggregates (> 1000 mm) favors dominance of 10 mm particles in the *Hyparrhenia* assemblage and 30 mm and 300 mm particles in the *Nastus* assemblage.

Dissolution creates cavities whose size increases with increasing time of exposure to the alkaline solution. ELONGATE, BLOCKY and BULLIFORM morphotypes exhibited more highly pitted surfaces in soils and sediments than SADDLES and RONDELS, a phenomenon observed elsewhere (e.g., Alexandre et al., 1999; Meunier et al. 1999, Osterrieth et al., 2009), perhaps because pits and cavities may be a feature of weathering that reflects a particular silica structure or density of various phytolith morphotypes. SAD, RON and BIL originate in silica cells, accumulating silica in the cell lumen, while ELO, BUL-FLA and BLO originate from cell walls and include a greater number of various organic molecules, likely weakening the silica structure (Kumar et al., 2016, 2017a, b).

4.2 Stability of phytoliths in soils and paleosols

Our finding that plant phytoliths dissolve more easily than soil and paleosol phytoliths (Fig. 3) is consistent with previous findings (Cabanes et al., 2011; Fraysse et al. 2009; Meunier et al. 2014), also observed for other biogenic silica particles such as diatoms that dissolve faster when compared to those extracted from sediments (Van Cappellen et al., 2002). Fraysse et al. (2006) showed that the specific surface area of phytoliths extracted from *Nastus* is 159.5 m^2g^{-1}, much higher than 5.18 m^2g^{-1} measured for La Réunion soil phytoliths (Fraysse et al., 2006). This difference likely results from transformation of the siliceous structure of phytoliths during pedogenesis, sedimentation or burial, leading to more resistance to dissolution. Unfortunately, we could not observe transformation of biogenic opal-A into more stable forms of amorphous silica (Kastner and Gieskes, 1983) in paleosol samples due to the dominance of quartz peaks in the XRD spectra. Al, commonly observed on soil phytolith surfaces (Bartoli and Wilding, 1980; Cornelis et al., 2011; Van Cappellen et al., 2002), detected on phytolith surfaces of paleosol samples (Fig. 1) may also decrease phytolith sensitivity to dissolution. Al deposition may occur during pedogenesis or sedimentation as suggested by Bartoli (1985), although Al has been detected in phytoliths extracted from plants (Carnelli et al., 2002). Finally, the low dissolution rate of paleosol phytoliths compared to plant and soil phytoliths may be accentuated by the presence of low solubility crystalline aluminosilicate and quartz particles remaining in the sample (Fraysse et al., 2009).

4.3 Assessment of phytolith-based paleo-environment reconstruction

We found that while the fragile silica particles almost totally disappeared (Fig. S2), relative abundances of the main phytolith types in an assemblage are not affected by dissolution (Fig. 6). This finding matches Cabanes and Shahack-Gross (2015), who showed that only double peaked husk, long cell wavy, parallelepipedal elongate rugulate phytoliths from rice inflorescences and papillates from sedges (fragile morphotypes not commonly preserved in soils) showed significant proportional change after partial dissolution, while relative abundances of morphotypes such as BULLIFORM and GSSCs remained constant. These results strongly indicate that past vegetation reconstructions from phytolith assemblages and phytolith indices are robust (Diester-Haass et al. 1973; Twiss, 1992).

La Reunion soils probably developed under long-term bamboo vegetation with *Nastus*

borbonicus as dominant species. Meunier et al. (1999) showed that RONDELS and SADDLES (named square and round in Meunier et al. (1999)) occurred in higher proportions in the leaves of *Nastus* compared to the surface soil, suggesting selective dissolution of these morphotypes. Yost et al. (2021) showed that GSSC phytoliths disappeared prior to ELONGATE and BULLIFORM phytoliths in a continuous sediment core from Lake Baringo, Kenya. They proposed a conceptual model for biogenic silica dissolution succession, suggesting that phytoliths, diatoms, and sponge spicules exhibit more cavities and even disappear when pH increases and also shows that short cells disappear at lower pH than BUL-FLA, BLO and ELO.

In our experiments, where we maintained pH at 11.2 (at 85 °C), all morphotypes including short cells, ELO, BLO and BUL-FLA are still present and some do not even show cavities (e.g., SPH). Proportions within the GSSCs and between GSSCs, ELO, BLO, and BUL-FLA are also maintained. Our study does not confirm selective dissolution of common phytolith morphotypes or the model of silica dissolution succession proposed by Yost et al (2021). However, if dissolution experiments had continued considerably longer, we cannot reject they may in fact have been able to confirm the model of Yost et al. (2021). Apart from dissolution, soil and sediment phytolith assemblages can be affected by physical erosion and selective translocation inside the soil column (Alexandre et al., 1997; Alexandre et al., 2011; Kaczorek et al., 2019). GSSCs with smaller volume are more easily translocated to deeper layers (Liu et al., 2019) and exported by erosion, likely explaining the over-representation of long and/or large particles in some sedimentary levels and soil layers.

Our results indicate that although dissolution kinetics differ between phytolith assemblages, relative proportions of phytolith morphotypes typically used for paleoenvironmental reconstruction stay stable. Phytolith assemblages showing dissolution features can still provide significant qualitative information. Other taphonomic processes such as translocation and erosion that may modify phytolith assemblages extracted from soils and sediments should be addressed in future studies.

Conclusion

Our systematic analysis, examining effects of partial alkaline dissolution on plant, soil and paleosol phytolith assemblages by considering phytolith surface features, assemblage changes and

Si release, shows that dissolution leads to formation of pits and cavities, an increase in number and size of cavities on phytolith surfaces, as well as rapid loss of thin silica particles such as silicified stomata cells and cell walls. The order of the dissolution rate of phytoliths is plant > soil > paleosol. Pedogenic and burial processes lead to stable phytolith assemblages. Dissolution does not significantly change relative proportions of stable phytolith morphotypes within an assemblage, supporting the robustness of past vegetation interpretations inferred from phytolith assemblages.

Acknowledgments

This research has benefited from the support of the China Scholarship Council through the provision of financial support to HL and the support of CEREGE APIC fund to DB and JDM for carrying the experiments. We thank Daniel Borschneck, Yves Noack, Baptiste Suchéras-Marx, Sandrine Conrod, Christine Pailles and Jean-Charles Mazur at CEREGE for their helpful contribution.

References

Alexandre, A., Bouvet, M., and Abbadie, L., 2011. The role of savannas in the terrestrial Si cycle: A case-study from Lamto, Ivory Coast. Global and Planetary Change 78, 162-169.

Alexandre, A., Meunier, J.D., Colin, F., Koud, J.M., 1997. Plant impact on the biogeochemical cycle of silicon and related weathering processes. Geochimica et Cosmochimica Acta 61, 677-682.

Alexandre, A., Meunier, J.D., Mariotti, A., Soubies, F., 1999. Late Holocene Phytolith and Carbon-Isotope Record from a Latosol at Salitre, South-Central Brazil. Quaternary Research 51, 187-194.

Aleman, J.C., Canal-Subitani, S., Favier, C., Bremond, L., 2014. Influence of the local environment on lacustrine sedimentary phytolith records. Palaeogeography, Palaeoclimatology, Palaeoecology 414, 273-283.

Arráiz, H., Barboni, D., Ashley, G.M., Mabulla, A., Baquedano, E., Domínguez-Rodrigo, M. 2017. The FLK Zinj paleolandscape: Reconstruction of a 1.84Ma wooded habitat in the FLK Zinj-AMK-PTK-DS archaeological complex, Middle Bed I (Olduvai Gorge, Tanzania), Palaeogeography, Palaeoclimatology, Palaeoecology 488, 9-20.

Ball, T., Chandler-Ezell, K., Dickau, R., Duncan, N., Hart, T.C., Iriarte, J., Lentfer, C., Logan, A., Lu, H., Madella, M., Pearsall, D.M., Piperno, D.R., Rosen, A.M., Vrydaghs, L., Weisskopf, A., Zhang, J., 2016. Phytoliths as a tool for investigations of agricultural origins and dispersals around the world. Journal of Archaeological Science 68, 32-45.

Bartoli, F., 1985. Crystallochemistry and surface properties of biogenic opal. The European Journal of Soil Science 36, 335-350.

Bartoli, F., Wilding, L.P., 1980. Dissolution of Biogenic Opal as a Function of its Physical and Chemical Properties. Soil Science Society of America Journal 44, 873-878.

Blecker, S., McCulley, R., Chadwick, O., Kelly, E., 2006. Biologic Cycling of Silica across a Grassland Bioclimosequence, Global Biogeochemical Cycles 20, GB3023.

Borrelli, N., Alvarez, M.F., Osterrieth, M.L., Marcovecchio, J.E., 2010. Silica content in soil solution and its relation with phytolith weathering and silica biogeochemical cycle in Typical Argiudolls of the Pampean Plain, Argentina-a preliminary study. Journal of Soils and Sediments 10, 983-994.

Bremond, L., Alexandre, A., Wooller, M.J., Hely, C., Williamson, D., Schafer, P.A., Majule, A., Guiot, J., 2008. Phytolith indices as proxies of grass subfamilies on East African tropical mountains. Global and Planetary Change 61, 209-224.

Cabanes, D., Shahack-Gross, R., 2015. Understanding fossil phytolith preservation: the role of partial dissolution in paleoecology and archaeology. PloS one 10, e0125532.

Cabanes, D., Weiner, S., Shahack-Gross, R., 2011. Stability of phytoliths in the archaeological record: a dissolution study of modern and fossil phytoliths. Journal of Archaeological Science 38, 2480-2490.

Carnelli, A.L., Madella, M., Theurillat, J.P., Ammann, B., 2002. Aluminum in the opal silica reticule of phytoliths: a new tool in palaeoecological studies, American Journal of Botany 89, 346-351.

Ciochon, R.L., Piperno, D.R., Thompson, R.G., 1990. Opal phytoliths found on the teeth of the extinct ape Gigantopithecus blacki: implications for paleodietary studies. Proceedings of the National Academy of Sciences, USA 87, 8120-8124.

Cordova, C.E., Johnson, W.C., Mandel, R.D., Palmer, M.W., 2011. Late Quaternary environmental

change inferred from phytoliths and other soil-related proxies: case studies from the central and southern Great Plains, USA. Catena 85, 87-108.

Cornelis, J.T., Delvaux, B., Georg, R.B., Lucas, Y., Ranger, J., Opfergelt, S., 2011. Tracing the origin of dissolved silicon transferred from various soil-plant systems towards rivers: a review. Biogeosciences 8, 89-112.

Crespin, J., Alexandre, A., Sylvestre, F., Sonzogni, C., Paillès, C., and Garreta, V., 2008. IR laser extraction technique applied to oxygen isotope analysis of small biogenic silica samples, Analytical Chemistry 80, 2372-2378.

Davis, J.C., 1986. Statistics and Data Analysis in Geology. John Wiley & Sons.

Diester-Haass, L., Schrader, H.J., Thiede, J., 1973. Sedimentological and palaeoclimatological investigations of two pelagic-ooze cores off Cape Barbas, North-West Africa. Meteor Forschungsergebnisse: Reihe, C., Geologie und Geophysik 16. pp. 19-66.

Fraysse, F., Pokrovsky, O.S., Schott, J., Meunier, J.D., 2006. Surface properties, solubility and dissolution kinetics of bamboo phytoliths. Geochimica et Cosmochimica Acta 70, 1939-1951.

Fraysse, F., Pokrovsky, O.S., Schott, J., Meunier, J.D., 2009. Surface chemistry and reactivity of plant phytoliths in aqueous solutions. Chemical Geology 258, 197-206.

Fredlund, G.G., Tieszen, L.L., 1994. Modern phytolith assem- blages from the North American Great Plains. Journal of Biogeography 21, 321-335.

Hammer, Ø., Harper, D.A.T., Ryan, P.D., 2001. PAST: paleontological statistics software package for education and data analysis. Palaeontologia Electronica 4, 1-9.

Hodson, M.J. 2019. The relative importance of cell wall and lumen phytoliths in carbon sequestration in soil: a hypothesis. Frontiers in Earth Science 7, 167.

Hodson, M.J., White, P.J., Mead, A., Broadley, M.R., 2005. Phylogenetic variation in the silicon composition of plants. Annals of Botany 96, 1027-1046.

Hyland, E., Smith, S.Y., Sheldon, N.D., 2013. Representational bias in phytoliths from modern soils of central North America: Implications for paleovegetation reconstructions. Palaeogeography, Palaeoclimatology, Palaeoecology 374, 338-348.

Iriarte, J., 2003. Assessing the feasibility of identifying maize through the analysis of cross-shaped size and three-dimensional morphology of phytoliths in the grasslands of southeastern South

America. Journal of Archaeological Science 30, 1085-1094.

Issaharou-Matchi, I., Barboni, D., Meunier, J.D., Saadou, M., Dussouillez, P., Contoux, C., Zirihi-Guede, N., 2016. Intraspecific biogenic silica variations in the grass species Pennisetum pedicellatum along an evapotranspiration gradient in South Niger. Flora-Morphology, Distribution, Functional Ecology of Plants 220, 84-93.

Kaczorek, D., Puppe, D., Busse, J., Sommer, M., 2019. Effects of phytolith distribution and characteristics on extractable silicon fractions in soils under different vegetation-An exploratory study on loess. Geoderma 356, 113917.

Kastner, M., Gieskes, J.M., 1983. Opal-A to opal-CT transformation: a kinetic study. Developments in Sedimentology 36, 211-227.

Kumar, S., Milstein, Y., Brami, Y., Elbaum, M., Elbaum, R., 2016. Mechanism of silica deposition in sorghum silica cells, New Phytologist 213, 791-798.

Kumar, S., Soukup, M., Elbaum, R., 2017a. Silicification in Grasses: Variation between Different Cell Types, Frontiers Plant Science 8, 438.

Kumar, S., Elbaum, R., 2017b. Interplay between silica deposition and viability during the life span of sorghum silica cells, New Phytologist 217, 1137-1145.

Lisztes-Szabó, Z., Filep, A.F., Csík, A., Pető, Á., Kertész, T.G., Braun, M., 2020. pH-dependent silicon release from phytoliths of Norway spruce (Picea abies). Journal of Paleolimnology 63, 65-81.

Liu, L., Li, D., Jie, D., Liu, H., Gao, G., Li, N., 2019. Translocation of phytoliths within natural Soil profiles in Northeast China. Frontiers in Plant Science 10, 1254.

Lu, H., Zhang, J., Liu, K.B., Wu, N., Li, Y., Zhou, K., Ye, M., Zhang, T., Zhang, H., Yang, X., Shen, L., Xu, D., Li, Q., 2009. Earliest domestication of common millet (Panicum miliaceum) in East Asia extended to 10,000 years ago. Proceedings of the National Academy of Sciences, USA 106, 7367-7372.

Lu, H., Zhang, J., Yang, Y., Yang, X., Xu, B., Yang, W., Tong, T., Jin, S., Shen, C., Rao, H., Li, X., Lu, H., Fuller, D.Q., Wang, L., Wang, C., Xu, D., Wu, N., 2016. Earliest tea as evidence for one branch of the Silk Road across the Tibetan Plateau. Scientific Reports 6, 18955.

McCune, J.L., Pellatt, M.G., 2013. Phytoliths of Southeastern Vancouver Island, Canada, and their

potential use to reconstruct shifting boundaries between Douglas-fir forest and oak savannah. Palaeogeography, Palaeoclimatology, Palaeoecology 383-384, 59-71.

Meunier, J.D., Colin, F., Alarcon, C., 1999. Biogenic silica storage in soils. Geology 29, 835-838.

Meunier, J.D., Cornu, S., Keller, C., Doris, B., 2022. The role of silicon in the supply of terrestrial ecosystem services. Environmental Chemistry Letters 20, 2109-2121.

Meunier, J.D., Keller, C., Guntzer, F., Riotte, J., Braun, J.J., Anupama, K., 2014. Assessment of the 1% Na_2CO_3 technique to quantify the phytolith pool. Geoderma 216, 30-35.

Neumann, K., Ball, T., Albert, R.M., Vrydaghs, L., Cummings, L.S., 2019. International Code for Phytolith Nomenclature (ICPN) 2.0. Annals of Botany 124, 189-199.

Nguyen, M.N., Dultz, S., Meharg, A.A., Pham, Q.V., Hoang, A.N., Dam, T.T.N., Nguyen, V.T., Nguyen, K.M., Nguyen, H.X., Nguyen, N.T., 2019. Phytolith content in Vietnamese paddy soils in relation to soil properties. Geoderma 333, 200-213.

Nogué, S., Whicher, K., Baker, A.G., Bhagwat, S.A., Willis, K.J., 2017. Phytolith analysis reveals the intensity of past land use change in the Western Ghats biodiversity hotspot, Quaternary International 437, 82-89.

Novello, A., Lebatard, A.E., Moussa, A., Barboni, D., Sylvestre, F., Bourlès, D. L., Paillès, C., Buchet, G., Decarreau, A., Duringer, P., Ghienne, J.F., Maley, J., Mazur, J.C., Roquin, C., Schuster, M., Vignaud, P., 2015. Diatom, phytolith, and pollen records from a $^{10}Be/^{9}Be$ dated lacustrine succession in the Chad basin: insight on the Miocene-Pliocene paleoenvironmental changes in Central Africa. Palaeogeography, Palaeoclimatology, Palaeoecology 430, 85-103.

Osterrieth, M., Madella, M., Zurro, D., Fernanda Alvarez, M., 2009. Taphonomical aspects of silica phytoliths in the loess sediments of the Argentinean Pampas. Quaternary International 193, 70-79.

Outrequin, C., 2022. The ^{17}O-excess of plant silica: towards a new humidity indicator Atmospheric Discipline Science. PhD thesis. Aix-Marseille University.

Piperno, D.R., Pearsall, D.M., 1998. The silica bodies of tropical American grasses: morphology, taxonomy, and implications for grass systematics and fossil phytolith identification. Smithsonian Contributions to Botany 85, 1-40.

Piperno, D.R., 2006. Phytoliths: a comprehensive guide for archaeologists and paleoecologists.

AltaMira Press, New York.

Prasad, V., Strömberg, C.A.E., Leache, A., Samant, B.R.P., Tang, L., Mohabey, D.M., Ge, S., Sahni, A., 2011. Late Cretaceous origin of the rice tribe provides evidence for early diversification in Poaceae.. Nature Communications 2, 480.

Riotte, J., Meunier, J.D., Zambardi, T., Audry, S., Barboni, D., Anupama, K., Prasad, S., Chmeleff, J., Poitrasson, F., Sekhar, M., Braun, J.J., 2018. Processes controlling silicon isotopic fractionation in a forested tropical watershed: Mule Hole Critical Zone Observatory (Southern India). Geochimica et Cosmochimica Acta 228, 301-319.

Rosen, A.M., Weiner, S., 1994. Identifying ancient irrigation: a new method using opaline phytoliths from emmer wheat. Journal of Archaeological Science 21, 125-132.

Saccone, L., Conley, D.J., Koning, E., Sauer, D., Sommer, M., Kaczorek, D., Blecker, S.W., Kelly, E.F., 2007. Assessing the extraction and quantification of amorphous silica in soils of forest and grassland ecosystems. European Journal of Soil Science 58, 1446-1459.

Suchéras-Marx, B., Escarguel, G., Ferreira, J., Hammer, Ø., 2019. Statistical confidence intervals for relative abundances and abundance-based ratios: Simple practical solutions for an old overlooked question. Marine Micropaleontology 151, 101751.

Twiss, P.C., 1992 Predicted world distribution of C3 and C4 grass phytoliths. In: Rapp G Jr, Mulholland SC (eds) Phytolith systematics: emerging issues. Plenum Press, New York, London, pp. 13-128.

Van Cappellen, P., Dixit, S., van Beusekom, J., 2002. Biogenic silica dissolution in the oceans: Reconciling experimental and field-based dissolution rates. Global Biogeochemical Cycles 16, 23-21-23-10.

White, A.F., Vivit, D.V., Schulz, M.S., Bullen, T.D., Evett, R.R., Aagarwal, J., 2012. Biogenic and pedogenic controls on Si distributions and cycling in grasslands of the Santa Cruz soil chronosequence, California. Geochimica et Cosmochimica Acta 94, 72-94.

Wilding, L.P., Drees, L.R., 1974. Contributions of Forest Opal and Associated Crystalline Phases to Fine Silt and Clay Fractions of Soils. Clays and Clay Minerals 22, 295-306.

WoldeGabriel, G., Ambrose, S.H., Barboni, D., Bonnefille, R., Bremond, L., Currie, B., DeGusta, D., Hart, W.K., Murray, A.M., Renne, P.R., Jolly-Saad, M.C., Stewart, K.M., White, T.D.,

2009. The geological, isotopic, botanical, invertebrate, and lower vertebrate surroundings of Ardipithecus ramidus. Science 326, 61-65.

Yost, C.L., Ivory, S.J., Deino, A.L., Rabideaux, N.M., Kingston, J.D., Cohen, A.S., 2021. Phytoliths, pollen, and microcharcoal from the Baringo Basin, Kenya reveal savanna dynamics during the Plio-Pleistocene transition. Palaeogeography, Palaeoclimatology, Palaeoecology 570, 109779.

Zhang, J., Lu, H., Jia, J., Shen, C., Wang, S., Chu, G., Wang, L., Cui, A., Wu, N., Li, F., 2020. Seasonal drought events in tropical East Asia over the last 60,000 y. Proceedings of The National Academy of Sciences, USA 117, 30988-30992.

Zhao, Z., Piperno, D.R., 2000. Late Pleistocene/Holocene environments in the Middle Yangtze River Valley, China and rice (Oryza sativa L.) domestication: the phytolith evidence. Geoarchaeology: An International Journal 15, 203-222.